Vegetation dynamic analysis based on multisource remote sensing data in the east margin of the Qinghai-Tibet Plateau, China

Wang Haijun [Corresp., 1, 2] , **Peng Peihao** [Corresp., 1] , **Kong Xiangdong** [2, 3] , **Zhang Tingbin** [1] , **Yi Guihua** [1]

[1] College of Earth Science, Chengdu University of Technology, Chengdu, Sichuan, China

[2] Engineering and Technical College of Chengdu University of Technology, Leshan, Sichuan, China

[3] School of Civil Engineering and Architecture, Southwest Petroleum University, Chengdu, China

Corresponding Authors: Wang Haijun, Peng Peihao
Email address: wanghaibo.2006@163.com, peihaop@163.com

This study focuses on the vegetation dynamic caused by global environmental change in the eastern margin of the Qinghai-Tibet Plateau (EMQTP). The Qinghai–Tibet Plateau (QTP) is one of the most sensitive areas responding to global environmental change, particularly global climate change, and has been recognized as a hotspot for coupled studies on changes in global terrestrial ecosystems and global climates. An important component of terrestrial ecosystems, vegetation dynamic has become a key issue in global environmental change, and numerous case studies have been conducted on vegetation dynamic trends using multi-source data and multi-scale methods across different study periods. The EMQTP is regarded as a transitional area located between the QTP and the Sichuan basin, and has special geographical and climatic conditions. Although this area is ecologically fragile and sensitive to climate change, few studies about vegetation dynamics have been carried out in this area. Thus, in this study, we used long-term series datasets of GIMMS 3g NDVI and VGT/PROBA-V NDVI to analyze the vegetation dynamics and phenological changes from 1982 to 2018. Validation was performed based on Landsat NDVI and Vegetation Index & Phenology (VIP) data. The results reveal that the year 1998 was a vital turning point in the start of growing season (SGS) in vegetation ecosystems. Before this turning point, the SGS had an average slope of 9.2 days/decade, and after, the average slope was 3.9 days/decade. The length of growing season (LGS) was slightly prolonged between 1982 to 2015. Additionally, the largest national alpine wetland grassland experienced significant vegetation degradation; in autumn, the degraded area accounted for 63.4%. Vegetation degradation had also appeared in the arid valleys of the Yalong River and the Jinsha River. Through validation analysis, we found that the main causes of vegetation degradation are the natural degradation of wetland grassland and human activities, specifically agricultural development and residential area expansion.

1 **Vegetation dynamic analysis based on multisource remote sensing data in the east**
2 **margin of the Qinghai-Tibet Plateau, China**

3 Haijun Wang[1, 2], Peihao Peng [1], Xiangdong Kong[2,3], Tingbin Zhang[1,2] and Guihua Yi[1]

4 [1] College of Earth Science, Chengdu University of Technology, Chengdu, Sichuan, China

5 [2] Engineering and Technical College of Chengdu University of Technology, Leshan, Sichuan, China

6 [3] School of Civil Engineering and Architecture, Southwest Petroleum University, Chengdu, China
7 Haijun Wang[1, 2] and Peihao Peng[1]
8 Chengdu, Sichuan Province, China
9 Email address: wanghaibo.2006@163.com, peihaop@163.com.

Abstract

11 This study focuses on the vegetation dynamic caused by global environmental change in the eastern
12 margin of the Qinghai-Tibet Plateau (EMQTP). The Qinghai–Tibet Plateau (QTP) is one of the most
13 sensitive areas responding to global environmental change, particularly global climate change, and has
14 been recognized as a hotspot for coupled studies on changes in global terrestrial ecosystems and global
15 climates. An important component of terrestrial ecosystems, vegetation dynamic has become a key issue
16 in global environmental change, and numerous case studies have been conducted on vegetation dynamic
17 trends using multi-source data and multi-scale methods across different study periods. The EMQTP is
18 regarded as a transitional area located between the QTP and the Sichuan basin, and has special
19 geographical and climatic conditions. Although this area is ecologically fragile and sensitive to climate
20 change, few studies about vegetation dynamics have been carried out in this area. Thus, in this study, we
21 used long-term series datasets of GIMMS 3g NDVI and VGT/PROBA-V NDVI to analyze the vegetation
22 dynamics and phenological changes from 1982 to 2018. Validation was performed based on Landsat
23 NDVI and Vegetation Index & Phenology (VIP) data. The results reveal that the year 1998 was a vital
24 turning point in the start of growing season (SGS) in vegetation ecosystems. Before this turning point, the
25 SGS had an average slope of 9.2 days/decade, and after, the average slope was 3.9 days/decade. The
26 length of growing season (LGS) was slightly prolonged between 1982 to 2015. Additionally, the largest
27 national alpine wetland grassland experienced significant vegetation degradation; in autumn, the
28 degraded area accounted for 63.4%. Vegetation degradation had also appeared in the arid valleys of the
29 Yalong River and the Jinsha River. Through validation analysis, we found that the main causes of
30 vegetation degradation are the natural degradation of wetland grassland and human activities,
31 specifically agricultural development and residential area expansion.

Introduction

33 Vegetation is the main component of terrestrial ecosystems on earth (Piao et al., 2003), playing a
34 crucial role in energy exchange, water cycles and biological cycles on the terrestrial surface. Vegetation
35 connects the atmosphere, hydrosphere and biosphere, and is vital for reducing greenhouse gases,
36 regulating carbon balance, and maintaining climate stability at the global scale (Hu et al., 2010).
37 Vegetation dynamics are especially sensitive to climate change (Yang and Piao, 2006) and, in recent years,
38 have been regarded as the key element in the global changes of terrestrial ecosystems (Kelly et al., 2011;
39 Li et al., 2019).

40   Because of its long-term series span and large area coverage, remote sensing data has become a
41   common and vitally important data source in the field of vegetation dynamics monitoring (Casa et al.,
42   2018). The normalized difference vegetation index (NDVI) is widely used as a parameter of vegetation
43   dynamics and refers to the quantitative values of vegetation conditions. It is often obtained through a
44   combination of different spectral remote sensing data. Due to its sensitivity to vegetation growth status,
45   phenology changes, and vegetation cover change (Tucker, 1979), NDVI has been the most widely applied
46   indicator used to represent vegetation status among various other vegetation indices. Global Inventory
47   Monitoring and Modeling Studies (GIMMS) 3g NDVI and SPOT VGEATION (VGT) NDVI have been
48   acknowledged as the most widely used remote sensing data products (Casa et al., 2018; Chavez et al.,
49   2019), being used to monitor vegetation dynamics at both regional and global scales (Liu et al., 2017; Wu
50   et al., 2016). GIMMS NDVI data cover a large time span from 1982 to 2015, and VGT NDVI has higher
51   spatial and temporal resolutions.

52   One of the most sensitive areas responding to global environmental change (Yang and Piao, 2006; Li
53   et al., 2019), the QTP has been recognized as a hotspot for vegetation dynamics. Peng et al. used the Hurst
54   exponent to analyze the trend of vegetation dynamics (Peng et al., 2012), and an eco-environmental
55   vulnerability change was performed in the Sanjiangyuan region of the QTP based on Liu's fuzzy analytic
56   hierarchy process (Liu et al., 2017). Shen and colleagues looked at the spring vegetation phenology
57   change in the QTP in the last decade (Shen et al., 2014), and the response of artificial vegetation to
58   changes in the ecological environment of the QTP was studied by Liu (Li et al., 2017). The EMQTP is a
59   transitional zone reaching from the Sichuan basin to the QTP (Li et al., 2019; Amelie et al., 2009). It
60   belongs in the Qinghai-Tibet Plateau climate zone and is affected by southeast monsoons. The largest
61   alpine wetland and natural pasture are located in the EMQTP, and alpine and subalpine meadows are the
62   dominant vegetation in this area. Additionally, this area contains the important Yangtze and Yellow
63   Rivers. This area has special conditions that make it suitable for the research of terrestrial ecosystems,
64   particularly wetland changes and vegetation dynamics. The terrestrial ecosystem of the QTP has also
65   transformed (Li et al., 2019; Fei et al., 2018) with the current backdrop of global climate change (IPCC,
66   2014). How has the terrestrial ecosystem, specifically the vegetation, of the EMQTP (a transitional and
67   special area) changed? The answer to this question has significant meaning for the ecological protection
68   of the river source area. However, few studies have focused on this area for vegetation dynamic research.
69   Previously, Peng analyzed vegetation change trends from 1982 to 2001, and tested the results by P values
70   in the QTP area (Peng et al., 2012). This was a well-executed study, but has two vital problems that need
71   to be discussed: first, the P value test may be unreliable since it is easy to pass (Chris, 2015), necessitating
72   the reevaluation of the significance of the vegetation change trend; second, the NDVI statistics for the
73   various vegetation were not described clearly. Were statistics taken at a site scale or at a regional scale?
74   This ambiguity brings into question the validity of the results.

75   In this work, we studied the EMQTP (a sub-area of the QTP) (Fig. 1) using multisource NDVI images
76   and a semi-innovative approach to analyze vegetation dynamic trends between 1982 to 2018. More
77   specifically, this study attempted to address the following questions:
78   (1) What was the multi-scale phenological change of the study area?
79   (2) What were the temporal-spatial dynamics of different vegetation?

80 2 Materials & Methodologies

81 2.1. Study area

82   The EMQTP (Fig. 1) extends from Hengduan Mountain to Qilian Mountain (26.1 – 36.2°E, 94.0 –

83 104.4°N). It includes the Ganzi, Aba autonomous prefecture of Sichuan province, and parts of Qinghai

84 Province and Tibet. This is the source region for some important rivers, such as Yangtze River and the

85 Yellow River. Moreover, this region is the largest natural pasture and has the largest alpine wetland

86 grassland in China, and alpine and sub-alpine meadows dominate this area. Frequent human activities

87 and climate changes in this area have caused transformations in the vegetation cover and degradation to

88 the grassland. This area has been defined as a typical ecologically fragile area by the government, and

89 accordingly needs to be researched and protected.

90 2.2. Image and processing

91 2.2.1. Image sources

92 (1) GIMMS 3g NDVI dataset

93   The most recent version of the Global Inventory Modeling and Mapping Studies (GIMMS) 3g NDVI

94 (NASA-NEX, 2019) (January 1982 to December 2015) by AVHRR sensor was the dataset used in this

95 study. The 3g data were produced in a geographical coordinate with a 15-day interval and a spatial

96 resolution of 0.083°×0.083° per pixel, and had been submitted to atmospheric and radiometric correction.

97 The 3g NDVI data were generated to improve the reliability for areas with short growing seasons (Zheng

98 et al., 2017; Florian et al., 2016; Du et al., 2015). The 3g NDVI data processed using MVC methods

99 generated monthly NDVI values. This process eliminated the effects of atmosphere, clouds, soil, and

100 snow. The 3g data were downloaded from ECOCAST (https://ecocast.arc.nasa.gov).

101 (2) SPOT VGT \PROBA-V NDVI dataset

102   Other long-term NDVI series datasets used in this study were the SPOT VGT (S10) and PROBA-V, a

103 10-day composite NDVI dataset taken at a spatial resolution of 1 x 1 km from the period of April 1998 to

104 October 2018. The quality of the VGT NDVI dataset in terms of geometry and radiometry processing for

105 directional and atmospheric effects marks it as an excellent instrument for monitoring forests, grasses,

106 and crops (VITO, 2018). Additionally, the PROBA-V NDVI (PROBA-V Products User Manual, 2018) data

107 at 1km resolution were also used in this study to extend the monitoring time. A PROBA-V satellite was

108 launched in May 2013 to plug the gap between SPOT-VGT and Sentinel-3 satellites. The two NDVI

109 datasets were generated using the MVC method (Holben,1986), as MVC was confirmed as a reliable and

110 practical method from many previous studies. The VGT\PROBA-V NDVI dataset has been used widely

111 in forest, grassland and crop dynamic studies largely due to its high quality (PROBA-V Products User

112 Manual, 2018). The data were downloaded from VITO Earth Observation (http://www.vito-eodata.be).

113 (3) Data Engine of VIP Lab.

114   The data engine of the VIP (Vegetation Index & Phenology) Laboratory provides phenology data at a

115 global range using a three-dimensional grid. The VIP product (VIP Lab, 2011) was generated based on the

116 AVHRR (Advanced Very High-Resolution Radiometer) dataset with a spatial resolution of 0.05° × 0.05°

117 per pixel. This is a yearly phenology product with a time span from 1982 to 2015. This product includes

118 the start of season, end of season, and the day of peak. VIP phenology products are available from the

119 Vegetation Index & Phenology Lab (https://vip.arizona.edu).

120 (4) Landsat NDVI

121   Landsat Thematic Mapper (TM) and Operational Land Imager (OLI) data were used to validate the
122   NDVI-based (GIMMS 3g and VGT\PROB-V) vegetation dynamic trends. The Landsat 5 (L5) image
123   consists of seven bands with a spatial resolution of 30 m. Band 3 (0.63-0.69 μm) is in the red (R) spectrum,
124   and band 4 (0.76-0.90 μm) is near the infrared red (NIR) spectrum. Landsat 8 (L8) OLI includes nine
125   bands with a spatial resolution of 30 m. Among them, Band 4 is in the R spectrum (0.63-0.68 μm) and
126   Band 5 is in the NIR spectrum (0.845-0.885 μm). We used NIR and R band to calculate NDVI, and
127   validation was performed based on this vegetation index. The study area is covered by a large number of
128   clouds, especially in summer, and we needed to select images with less than 5% clouds from the USGS
129   website. The basic information of the images downloaded, including the orbital number, sensor type, and
130   image acquisition date, are shown in Table 1.
131   (5) Vegetation and topographic maps
132   The vegetation vector map is at 1: 100000 scale. Global Land Cover 2015 raster data and terrain data
133   (SRTM-DEM) of the study area have a spatial resolution of 30m, and they are available from the USGS
134   database (https://earthexplorer.usgs.gov/).
135   2.2.2 Data processing
136   Step 1. Smoothing processing of NDVI images
137   A simplified least squares-fit convolution was proposed by Savitzky and Golay in order to smooth
138   and compute derivatives of a set of consecutive spectrum values (Cao et al., 2018; Savitzky and Golay,
139   1964). The convolution can be recognized as a weighted moving average filter, with weight allocated as a
140   polynomial of a certain form. We can apply the filter to any consecutive data when data points are at a
141   fixed and uniform interval along the chosen abscissa, and the curves formed by graphing the points must
142   be continuous and smooth. The long-term series GIMMS 3g NDVI and SPOT VGT NDVI just satisfy these
143   conditions. The general equation of the simplified least-squares convolution for NDVI time-series
144   smoothing is as follows:

145     $$NDVI_j^* = \frac{\sum_{i=-m}^{i=m} C_i NDVI_{j+i}}{N} \text{ , (1)}$$

146   Where $NDVI$ is the raw pixel value, $NDVI^*$ is the pixel smoothed value, C_i is the coefficient for the ith
147   NDVI value of the filter, and N is the number of convoluting integers. It is equal to the smoothing
148   window size (2m + 1). The index j is the running index of the original ordinate data table. The smoothing
149   array (filter size) consists of 2m + 1 points, where m is the half-width of the smoothing window. The
150   coefficients of a Savitzky– Golay filter (C_i) are directly available from the latest version (Madden, 1978;
151   Savitzky and Golay, 1964; Steinier, et al., 1974).
152   Step 2. Co-registration of NDVI images
153   The coordinates of the downloaded raw images showed some deviations because they were imaged
154   with different sensors. In order to better analyze the data, especially the four types of images of the same
155   area, we needed to make a geometric co-correction. In light of the large difference in the spatial resolution
156   of images, the co-registration method based on image-to-image was performed for GIMMS 3g NDVI,
157   VGT/PROBA-V, and Landsat NDVI. We selected the same geo-features, such as rivers, lakes, and
158   mountains, to correct the images. The accuracy of this correction method is higher than the point-to-point
159   method based on ground control points (GCP).
160   Step 3. Sampling and statistics

161 (1). Image sampling

162   Sampling is indispensable when finding the trend analysis of NDVI at the site scale. The location and
163 the size of the sample especially will impact the results of NDVI trend analysis. Many factors were
164 considered, such as the sample being an area of vegetation cover, and only using the single type of
165 vegetation. Moreover, mixed pixels were eliminated for NDVI data with two different resolutions. Using
166 the analysis above, we selected 15 representative sample sites, with a sample size of 8 km x 8 km (GIMMS
167 3g NDVI, 1 x 1 pixel. VGT\PROBA-V NDVI, 8 x 8 pixels). The 15 sample sites selected were Songpan
168 (SP), Kangding (KD), Litang (LT), Jiuzhi (JZ), Derong (DR), Nangqian (NQ), Tongren (TR), Dege (Dege),
169 Ruoergai (REG), Maerkang (MEK), Ruobei (RB), Zeku (ZK), Gongshan (GS), and Yanyuan (YY). The
170 location and vegetation types of each site are shown in Table 2 and Fig. 2.

171 (2). Sample statistics

172   The basic principle of the sample statistics (Fig. 3) is that the calculation of pixel parameters was
173 performed by setting a zonal window with a fixed size. The calculated parameters included the sum,
174 mean, maximum, and minimum of the pixel values in the zonal window. The size of the zonal window
175 was set to 8 km x 8 km according to the lower resolution of the two different NDVI images in this study.
176 The results were divided into three cases (possibilities) for GIMMS 3g images, using the mean statistics of
177 a GIMMS 3g image as an example. The formulations are as follows.

178 $$Case_1: Mean = V_1 \, or \, V_2 \, or \, V_3 \, or \, V_4, \text{ (2)}$$

179 $$Case_2: Mean = \frac{V_1 + V_2}{2} \, or \, \frac{V_1 + V_3}{2} \, or \, \frac{V_2 + V_4}{2} \, or \, \frac{V_3 + V_4}{2}, \text{ (3)}$$

180 $$Case_3: Mean = \frac{V_1 + V_2 + V_3 + V_4}{4}, \text{ (4)}$$

181 Where V is the pixel value of GIMMS 3g NDVI images. According to this principle, the formula above
182 was additionally followed for VGT/PROBA-V NDVI image statistics. Due to its higher resolution, more
183 pixels were counted than in GIMMS NDVI images. Compared to the Point to Value Method (PVM), this
184 method provides more accurate statistical results and reduces invalid values.

185 **2.2. Methodologies**

186 2.2.1. Detection of phenological change

187   Previous studies (Chandola et al., 2010; Chu et al., 2018; Gu et al., 2018; Tang et al., 2018) have used
188 the dynamic threshold method to define the start of the growing season (SGS), the end of the growing
189 season (EGS), and the length of the growing season (LGS). This method defines SGS and EGS as the
190 moment when the pixel values increase and decrease, respectively, to a certain proportion of NDVI
191 amplitude in one year. This method can avoid the mutual interference caused by different regional water-
192 heat conditions, vegetation, and soil types in the fixed threshold method. The specific formulation is as
193 follows:

194 $$D_{SGS, \; EGS} = (NDVI_{max} - NDVI_{min}) \times C, \text{ (5)}$$

195 Where $NDVI_{max}$ is the maximum value and $NDVI_{min}$ is the minimum value of NDVI in one year. C is the
196 threshold ratio. According to previous studies (Yu et al., 2010; Jonsson et al., 2002) and the annual
197 variation of vegetation in the study area, the SGS and EGS thresholds were set at 20% in the sample site.
198 D is a time judgment function where the time point is taken as EGS or SGS when NDVI increases or
199 decreases to the threshold C. The time span from SGS to EGS is the LGS.

200 2.2.2. Trend analysis of the NDVI change

201   The stability and accuracy of the trend analysis method have been tested and it is widely used (Chu
202 et al., 2018; Gu et al., 2018; Tang et al., 2018). This method was applied at a pixel scale in the period 1982–
203 2018 to detect NDVI change and distribution. The formula is:

204
$$slope = \frac{n \times \sum_{i=1}^{n}(i \times NDVI_i) - \sum_{i=1}^{n}i\sum_{i=1}^{n}NDVI_i}{n \times \sum_{i=1}^{n}i^2 - (\sum_{i=1}^{n}i)^2}, (6)$$

205 where i is the number of the year, with the range 1 to n (GIMMS NDVI, n =34; VGT NDVI, n =20). $NDVI_i$
206 represents the growing season NDVI of year i. The slope is the trend in NDVI from 1982 to 2018. A *slope* >
207 0 indicates an increasing trend, while a *slope* < 0 represents a decreasing trend during the study period.

208 2.2.3. Mann-Kendall trend test

209   The Mann-Kendall (M-K) trend test has been widely used as a non-parametric statistical test method
210 (Gocic, et al., 2013; Yavuz, 2018). This test method does not require samples for normal distribution, and
211 it has a high degree of quantification. This method is suitable to trend test time series data, especially the
212 data of long-term series. The principles of the M-K trend test are as follows.

213
$$S_k = \sum_{i=1}^{k}r_i, k = 2, 3\cdots, n \qquad (5)$$

214
$$r_i = \begin{cases} +\ 1 & x_i > x_j \\ +\ 0 & x_i < x_j \end{cases} \quad j = 1,2\cdots, i \qquad (6)$$

215 Where n is the number of the sample, and x is the time span. s_k is the cumulative number of values at the
216 time i, greater than those at the time j.

217
$$UF_k = \frac{|S_k - E(S_k)|}{\sqrt{var(S_k)}}, k = 1, 2\cdots, n \qquad (7)$$

218
$$\begin{cases} E(S_k) = \frac{k(k-1)}{4} \\ var(S_k) = \frac{k(k-1)(2k+5)}{72} \end{cases}, k = 2,3,\cdots n \qquad (8)$$

219 Where UF_k is a statistic calculated by $x_1, x_2, \cdots x_n$. $E(S_k)$, and $var(S_k)$ is the mean and variance of S_k. UB_k=
220 $- UF_k(k = n, n - 1,\cdots,1)$, UB_1=0. a is the signification level. If $a = 0.05$, then the $u_{0.05} =\pm 1.96$.
221 A $UF_k > 0$ indicates an increasing trend, while a $UF_k < 0$ represents a decreasing trend. When the critical
222 line is exceeded ($u_{0.05} =\pm 1.96.$), a significant upward or downward trend is shown.

223 2.2.4. Bayesian trend test

224   The traditional approach of trend analysis cannot detect the turning point for a set of data in a time
225 series, and cannot estimate the change after it happens. The Bayesian method can overcome these
226 difficulties. The Bayesian theorem constructed the probability distribution (posterior probability) function
227 of the turning point of data change trends. The specific formula is:

228
$$P(\theta \mid data) = \frac{P(data \mid \theta) \times P(\theta)}{P(data)}, \qquad (9)$$

229 Where $P(\theta)$ denotes the prior probability distribution. $P(\theta \mid data)$ is the posterior probability distribution,
230 representing the confidence level of a turning point of change trends. $P(data)$ indicates the evidence;
231 more importantly, it indicates the moment of data peak. For example, in a set of data in time series X =
232 {$x_{1982}, x_{1983}, x_{1984} \cdots x_{2015}$}, how do the data change? We would need to calculate the moment and the
233 probability of the turning point occurring when the trend changes. We referred to previous studies
234 (Hèou, et al., 2017; Peter, et al., 2018; Zhao, et al., 2019; John, et al., 2015) to calculate the moment and

235 probability of the turning point occurring (Fig. 4). The combination of the Bayesian approach and M-K
236 trend analysis can improve the accuracy of trend analysis, and can validate M-K trend analysis. The
237 flowchart of methodology used in this study is shown in Fig. 5.

238 3 Results

239 **3.1. GIMMS 3g NDVI-based vegetation dynamic trends from 1982 to 2015**
240 3.1.1. Phenological trends of vegetation
241   The dynamic threshold method was used to detect the phenological changes of three ecosystems
242 from 1982 to 2015. The trend of phenology change (Fig. 6A, B, C, G, H, and I) and the M-K trend test (Fig.
243 6D, E, F, J, K, and L) are shown in Fig. 6. In the forest ecosystem (Fig. 6A and Fig. 6E), the SGS change
244 trend rose (*slope* = 10.08 days/decade, *UF* < 0, *Sig.* =0.05), and then began to fall (*slope* = 2.06 days/decade,
245 *UF* > 0, *Sig.* =0.05), showing overall trending delays (*slope* = 0.66 days/decade). The EGS showed a slight
246 decline from 1982 to 2015 (*slope* = 0.15 day/decade), although it began to advance after 1998 (*slope* = 0.89
247 day/decade). It was calculated that the LGS decreased by 0.51 days/ decade based on the SGS and EGS
248 during the study period. The curves of the SGS and EGS for grassland ecosystems are shown in Fig. 6C
249 and Fig. 6I. The SGS of the grassland ecosystem was accelerated by 0.64 days/decade, and the EGS was
250 delayed by 0.46 days/ decade. Accordingly, the LGS was prolonged by 1.1 days/decade from 1982 to 2015.
251 The variation trend of SGS in the grassland ecosystem was consistent with that of the forest ecosystem.
252 The year 1998 was the turning point of the curve, and after that year, the SGS curve showed trending
253 delays (*slope*= 2.68 days/ decade). For the farmland ecosystem (Fig. 6A and Fig. 6G), the trend of change
254 was consistent with that of the grassland and forest ecosystem, except for the change rate of SGS. From
255 1982 to 2015, the SGS trend was accelerated by 2.98 days/decade, and the EGS was delayed by 1.07
256 days/decade. Due to the acceleration of the SGS and the delay of the EGS, the LGS was prolonged by 8.74
257 days/decade (1982-2015).
258 3.1.2 Spatial dynamics of vegetation
259   We calculated the trend and spatial distribution of NDVI changes across different seasons from 1982
260 to 2015 (Fig. 7). In spring (Fig. 7A), the trend range of NDVI change was from -0.0679/decade to
261 0.0693/decade. Vegetation increased most in the area with a percentage of 82.1%, and were mainly
262 distributed in SP, GS, YY, REG and MEK. The needle-leaf deciduous forest showed vigorous activity in
263 SP, GS, and YY, and the vegetation coverage of swamp and plain grassland also experienced an upward
264 trend in REG and MEK. The vegetation dynamics showed a weak upward trend in DR, JZ, and NQ. The
265 slope was 0.005/decade to 0.013/decade in the alpine and subalpine meadows distributed in this area. In
266 addition, vegetation deterioration had occurred in regions of the EMQTP, such as the west of ZK and DR.
267 The west of DR was especially affected, as it is a desert grassland with low vegetation coverage. As
268 shown in Fig. 7B, summer vegetation experienced great degradation with more than 51.5% of the area
269 showing a downward trend. In particular, the south section of the study area had a slope of 0.08 / decade.
270 The proportion of the vegetation increase area was 71.7%, and was mainly distributed in NQ and DG
271 regions due to the degeneration of desert grassland. The vegetation dynamic in autumn (Fig. 7C) was
272 basically consistent with the mean trend of the full growing season (Fig. 7D). The area of NDVI increase
273 accounted for 75.1% in the full growing season. The difference between autumn and the growing season
274 is only shown in the slope rate of NDVI increase and decrease. In the growing season, the slope was -

275   0.0394/decade to 0.0486/decade. The maximum value appeared in RE, the south of SP, and the central
276   region of the study area. Through the analysis of vegetation dynamics across different seasons, we found
277   that the decrease of NDVI was mainly distributed in the western DR region and near the dry valley in the
278   south of the study area. The areas with obvious increases were distributed in the east section of the study
279   area. Because the EMQTP is a sub area of QTP, the spatial distribution of vegetation change provided a
280   quantitative value that could be compared with Peng's results (Fig. 7 of Peng's work). Although the time
281   ranges of NDVI were greatly different (1982-2003 and 1982-2015), they can better reflect the decreasing
282   trend of vegetation in the arid valley.

283   **3.2. VGT\PROBA-V NDVI-based vegetation dynamic trend from 1999 to 2018**

284   3.2.1. Phenological trends of vegetation

285   We used the VGT\PROBA-V NDVI with a fine resolution to calculate phenological trends. The
286   change detection of the SGS and EGS were performed on the most recent 19 years. The trend of SGS
287   change for the forest ecosystem showed delay (*slope* = 0.66 days / decade, -1.96 < *Sig.* < 1.96), and the EGS
288   showed a slight advanced trend (*slope* = 2.99 day/decade, UF < 0, -1.96 < *Sig.* < 1.96). Thus, it was
289   calculated that the LGS decreased by 3.65 days/decade during this period. The SGS and EGS curves for
290   the grassland ecosystem are shown in Fig. 8C and Fig. 8G. The SGS of the grassland ecosystem was
291   delayed by 0.92 days/decade, and the EGS was delayed by 1.05 days/ decade. Accordingly, the LGS was
292   prolonged by 0.03 days/decade. Compared with the forest ecosystem, the grassland ecosystem showed an
293   obvious uptrend. In the farmland ecosystem (Fig. 8A and Fig. 8D), the SGS was delayed by 5.76
294   days/decade and the EGS was delayed by 0.67 days/decade. Due to the delays of the SGS and the EGS,
295   the LGS was shortened by 5.09 days/decade.

296   3.2.2 Spatial dynamics of vegetation

297   In the most recent 19 years (1999-2018), NDVI showed a decreasing trend with the area accounting
298   for 63.4% in spring (Fig. 9A). Most was grassland cover area with a slope less than 0.004/decade.
299   Moreover, NDVI had decreased significantly in the eastern and southern dry valleys of the study area.
300   This area was covered by forest, especially obvious in the east of REG, south MEK, and the northwestern
301   section of KD. The areas of NDVI increase in summer (Fig. 9B), autumn (Fig. 9C), and the growing season
302   (Fig. 9D) were 71.8%,60.9% and 65.4%, respectively. The slopes of NDVI increase and decrease were
303   similar and the distribution area was roughly consistent. Compared with the spatial distribution of NDVI
304   changes from 1982 to 2015, a large area near REG showed some obvious differences. This area was
305   covered by alpine and sub-alpine meadows, and NDVI showed a downward trend with a slope of about
306   0.005/decade, especially in the summer (Fig. 9B). This indicated that vegetation degradation in the NEG
307   region has been more noticeable in the last 19 years, and more attention should be paid to the changes in
308   the ecological environment of this area.

309   **3.3. Crossing analysis of the vegetation dynamic from 1999 to 2015**

310   We used GIMMS 3g NDVI and VGT\PROBA-V NDVI to perform trend analysis across different
311   seasons between 1999 and 2015. The vegetation dynamics reflected the change trend and spatial
312   distribution of vegetation. We divided the vegetation dynamics into three categories (decrease, weak
313   change, and increase) according to the trend ratio of vegetation, ultimately creating the vegetation
314   dynamic map (Fig. 10). GIMMS 3g NDVI's general change trend was basically consistent with the results
315   that used VGT\PROBA-V NDVI. Evidently, the spatial distribution of vegetation dynamics using

316 VGT\PROBA-V NDVI appeared finer than the results using GIMMS 3g NDVI. Vegetation degradation
317 areas were mainly distributed in the REG grassland region and the arid valley regions of the Jinsha River
318 and Yalong River. The areas with high vegetation activity appeared in the southeast of MEK and the
319 south section of the study area, which included GS and YY.

320   In order to more deeply analyze the vegetation dynamic, we calculated the trend of each vegetation
321 type at a site scale (Fig. 11). As can be seen in Fig. 11 A - H, most of the vegetation showed an upward
322 trend, while the AM (DR, NQ and JZ site) showed a downward trend. This result was consistent with the
323 vegetation dynamics shown in Fig. 11 A and B. In addition, there were some differences between the two
324 data analysis results, such as the change trend of TM vegetation, caused by the spatial resolution of the
325 two datasets. In autumn, WL (MEK site), AM (DR, NQ and JZ site), and PG (REG site) showed a
326 downward trend with different slopes. The downward trend of PG (REG site) was the most significant,
327 and was also reflected in the vegetation dynamic distribution map (Fig.10C and G). For the full growing
328 season, the change trend of the seven cover types experienced an upward trend based on two NDVI
329 image products. Compared with Peng's research results (Fig. 6 of Peng's work), the analysis at the site
330 scale objectively reflects the NDVI change trend of the local area. It represents the change trend of various
331 vegetation changing with the environment, rather than just a simple average of the different regions.

332 ## 4 Discussion

333 **4.1. Validation of the phenological changes**

334   We used the M-K method to achieve the general trend of phenological changes in sub section 3.3.1.
335 In order to better detect the change trend across different phases, Bayesian trend analysis was performed
336 to obtain continuous probability and the turning points of the trend change from 1982 to 2015. The results
337 of our calculations are shown in Fig. 12. In regard to the change trend of the SGS, the turning point was in
338 1998 and the probability of occurrence was more than 0.5. The turning point of the change trend in forests
339 (Fig.12 B) was consistent with the M-K analysis results (Fig. 6E). Moreover, the change trend of the SGS
340 was divided into two phases: before and after the turning point in 1998. Before 1998, SGS showed a
341 downward trend, and the value of beta occurred continuously. SGS showed an upward change trend
342 after the turning point. However, there was neither an obvious change trend nor turning point (the
343 higher probability) for the EGS.

344   We selected the SGS (A-1982, B-1998, and C-2015) and EGS images of the VIP grid (D-1982, E-1998,
345 and F-2015) to validate the phenology change from 1982 to 2015. SGS and EGS images of VIP in 1982,
346 1998, and 2015 can be seen in Fig. 13. The location of the sample site (Table 1) was used to extract the
347 phenology change of vegetation based on VIP images in this study. Then the extracted data were used to
348 validate the phenology changes of the SGS and EGS. The validation results are shown in Fig. 14. The
349 overall trend of phenology change of VIP was consistent with that of GIMMS. In the analysis of section
350 3.1, we found that the phenology change showed an advanced trend before 1998, and then appeared to
351 delay until 2015. This turning point of phenology change was also seen in the SGS change of VIP V4.

352   We also analyzed previous studies on phenology change in this area and nearby regions. Before
353 1998, the turning point of phenology change, the SGS showed an obvious advanced trend with an
354 average slope of 10 days/decade (UF < 0, -1.96 < Sig. < 1.96) for various vegetation ecosystems. This was
355 basically consistent with the results of other relevant research, which found that the slope of SGS ranged

356 from 3.5 to 10.2 days/decade using various method and sub-areas (Zhang et al.,2013; Shen et al., 2014;
357 Piao et al., 2011; Kong et al., 2017). Many scholars have found 1998 as the approximate turning point of
358 SGS in the QTP, which is highly consistent with the result of this study (Piao et al., 2011; Shen et al., 2016).
359 The SGS showed a delay trend after 1998, and the delays calculated by GIMMS 3g and VGT NDVI were
360 1.8 days/decade and 0.7 days/decade, respectively, but the significance (Sig.) was greater than 0.05 in the
361 EMQTP. Currently, the trend of SGS change in the QTP after 1998 is a controversial topic (Zhang et al.,
362 2013; Yu et al., 2010; Shen et al., 2013). In this study, the average EGS of vegetation ecosystem was
363 delayed by 1 day/decade between 1982 and 2018. This is consistent with Che's finding (Che et al., 2014)
364 that the phenological change trend of the QTP at the end of the growing season was not guaranteed
365 (*slope*=0.96 day/decade).

366 **4.2. Validation of the vegetation dynamics**

367 The analysis of section 3.2 and 3.3 show that vegetation degradation has been obvious in the REG
368 area, especially in the last 20 years. Thus, the validation of vegetation dynamics in this area was
369 performed based on the Landsat NDVI. Because the most significant degradation appears in autumn, we
370 used autumn Landsat NDVI to validate the vegetation dynamics. Because of the quality (the cloud was
371 less than 5%) of the Landsat orthophoto, the 10 scenes selected were mainly from September and October,
372 and the time difference was less than a week. Moreover, we designed five sites to make the results of the
373 validation more intuitive. The validation results can be seen in Fig. 15. Although the resolutions of
374 VGT\PROBA-V NDVI (1 km) and Landsat NDVI (30 m) were different, the general vegetation dynamic
375 trends were fundamentally consistent (Fig. 15A and Fig. 15B). In particular, the validation sites showed
376 significant downward trends, indicating our previous calculations (sub-section 3.2) of vegetation
377 degradation were correct. In the circle image (the zoom view of the validation site), the vegetation
378 dynamic is due to the degradation of the alpine meadow (Site 1 and Site 2). Additionally, human
379 activities, such as changing farmland area (Site 4) and the expansion of residential areas (Site 3 and Site 5)
380 also have an impact on vegetation degradation. Previous studies have revealed the degradation of alpine
381 wetland meadows in the REG area, including the shrinkage of meadows (Li et al., 2015), ecological
382 degradation (Shen et al., 2019), and an increase of cultivated land (Rong et al., 2010). The validation
383 results in section 3 showed that vegetation dynamics and change trends are reasonable and credible.
384 Other previous works (Chen, 2018; Bian et al., 2017) have also proven the vegetation degradation in REG
385 area, and that the reason for vegetation degradation in the dry valley near the southern section isrelated
386 to climate change (Wang, et al., 2018).

387 **5 Conclusions**

388 We combined the high spatial resolution of Landsat NDVI with the long temporal span of GIMMS 3g
389 NDVI and VGT/PROBA-V NDVI to establish a 37-year record of vegetation dynamics in the EMQTP at
390 1km and 8km spatial resolution. Our research focused on the phenological change of vegetation
391 ecosystems, the trends of change, and fluctuation characteristics for various vegetation types in this
392 sensitive area responding to global environmental change. The acquired findings on vegetation dynamics
393 in the EMQTP, particularly in phenological changes and fluctuation characteristics for various vegetation
394 types, can be summarized as follows:

395 (1). The SGS of vegetation ecosystems advanced from 1982 to 1998, and then experienced trending
396 delays until 2018. The average advanced slope and delayed slope were 11.51 days/decade and 3.86
397 days/decade, respectively. The LGS of the vegetation ecosystem was prolonged with an average
398 value of 4.24 days/decade, and the LGS of the farmland ecosystem showed the most significant
399 prolongation trend.

400 (2). In the full growing season, the slope of the vegetation index (NDVI) ranged from -0.039/decade
401 to 0.049/decade. Most of this area showed an upward trend with a percentage of 75.1%. When
402 compared with the forest ecosystem, the grassland ecosystem showed weaker activity and the
403 appearance of degradation, particularly in spring and autumn.

404 (3). In the most recent 19 years, vegetation has degenerated in REG and the arid valley region of the
405 Jinsha River and Yalong River. This finding has also been confirmed by Landsat NDVI. Vegetation
406 degradation is due to the shrinking of alpine meadows and the impact of human activities, which
407 include the change of farmland area and the expansion of residential areas.

408 Acknowledgements

409 We thank VITO, ECOCAST, Global Inventory Modeling and Mapping Studies (GIMMS), and WESTDC
410 for the freely downloadable VGT\PROBA-V and GIMMS 3g NDVI datasets, SRTM DEM, and vegetation
411 vector map products, respectively. We would also like to thank the anonymous reviewers for their
412 constructive and detailed comments.

413 REFERENCES

414 **A. de la Casa, G. Ovando, L. Bressanini, J. Martinez, G. Diaz, C. Miranda, 2018**. Soybean crop coverage
415 estimation from NDVI images with different spatial resolution to evaluate yield variability in a plot.
416 ISPRS J. Photogram. 146: 531-547. DOI 10.1016/j.isprsjprs.2018.10.018.

417 **Amelie, V., David R.J., Francis, R., Jean, P.Q., Qiu, J.M., Qian, W., Li, T.Y., Nadine, B., Michael, C.,**
418 **Pierre, D., Kenichi, T., Weidmann, J.C., Patric, G., 2009.** Modelling and spatial discrimination of
419 small mammal assemblages: An example from western Sichuan (China) Ecological Modelling, 220,
420 1218-1231. DOI 10.1016/j.ecolmodel.2009.02.019.

421 **Bian, J.H., Li, A.N., Zhang, Z.J., 2017.** Monitoring fractional green vegetation cover dynamics over a
422 seasonally inundated alpine wetland using dense time series HJ-1A/B constellation images and an
423 adaptive endmember selection LSMM model. Remote Sens. Environ. 197: 98–114. DOI
424 0.1016/j.rse.2017.05.031.

425 **Cao, R.Y., Chen, Y., Shen, M.G., Chen, J., Wang, W.Y., 2018.** A simple method to improve the quality of
426 NDVI time-series data byintegrating spatiotemporal information with the Savitzky-Golay filter.
427 Remote Sensing of Environment,217,244-257. DOI 10.1016/j.rse.2018.08.022.

428 **Casa, A., Ovando, G., Bressanini, L., Martinez, J., Diaz, G., Miranda, G., 2018.** Soybean crop coverage
429 estimation from NDVI images with different spatial resolution to evaluate yield variability in a plot.
430 ISPRS journal of photogrammetry and remote sensing, 146,531-547. DOI
431 10.1016/j.isprsjprs.2018.10.018.

432 **Chandola, V., Hui, D., Gu, L., Bhaduri, B. and Vatsavai, R.R., 2010.** Using time series segmentation for
433   deriving vegetation phenology indices from MODIS NDVI data, Data Mining Workshops (ICDMW),
434   2010 IEEE International Conference on. IEEE, Sydney, Australia, 202-208.

435 **Chavez, R.O., Moreira-Munoz, A., Galleguillos, M., Olea, M., Aguayo, J., Latin, A., Aguilera-Betti, I.,**
436   **Munoz, A.A., Manriquez, H., 2019.** Int J Appl Earth Obs Geoinformation, 76,193-203. DOI
437   10.1016/j.jag.2018.11.013.

438 **Che, M., Chen, B., Innes J L., 2014.** Spatial and temporal variations in the end date of the vegetation
439   growing season throughout the Qinghai-Tibetan Plateau from 1982 to 2011. Agr. Forest Meteorol.
440   189/190: 81-90. DOI 10.1016/j.agrformet.2014.01.004.

441 **Chen, J. L., 2018.** Analysis on vegetation change and driving factors in the alpine plateau of REG. Sichuan
442   Normal University, Master Dissertation. 1-63.

443 **Chris, W., 2015.** Psychology journal bans P values. Nature, 7541 (519). DOI:10.1038/519009f.

444 **Chu, H.S., Sergey Venevsky, Wu, C., Wang, M.H., 2018.** NDVI-based vegetation dynamics and its
445   response to climate changes at Amur-Heilongjiang River Basin from 1982 to 2015. Sci. Total Environ.
446   650: 2051-2062. DOI 10.1016/j.scitotenv.2018.09.115.

447 **Du, J.Q., Shu, J.M., Yin, J.Q., Yuan, X.J., Ahati Jiaerheng, Xiong, S.S., He, P., Liu, W.L., 2015.** Analysis
448   on spatio-temporal trends and drivers in vegetation growth during recent decades in Xinjiang,
449   China. Int. J. App. Earth Obs. 38: 216-228. DOI 10.1016/j.jag.2015.01.006.

450 **Fei P., Xian, X., You, Q.G., Huang, G.H., Dong, S.Y., Liao, J., Duan, H.C., Atsushi, T., Wang, T., 2018.**
451   Changes of soil properties regulate the soil organic carbon loss with grassland degradation on the
452   Qinghai-Tibet Plateau. Ecological Indicators 93, 572–580. DOI 10.1016/j.ecolind.2018.05.047.

453 **Florian Detsch, Insa Otte, Tim Appelhans, Andreas Hemp, Thomas Nauss, 2016.** Seasonal and long-
454   term vegetation dynamics from 1-km GIMMS-based NDVI time series at Mt. Kilimanjaro, Tanzania.
455   Remote Sens. Environ. 178: 70-83. DOI 10.1016/j.rse.2016.03.007.

456 **Gocic M., Trajkovic S., 2013.** Analysis of changes in meteorological variables using Mann-Kendall and
457   Sen's slope estimator statistical tests in Serbia. Global and Planetary Change,100, 72-182. DOI
458   10.1016/j.gloplacha.2012.10.014.

459 **Gu, Z.J., Duan, X.W., Shi, Y.D., Li, Y., Pan, X., 2018.** Spatiotemporal variation in vegetation coverage and
460   its response to climatic factors in the Red River Basin, China. Ecol. Indic. 93:53-64. DOI
461   10.1016/j.ecolind.2018.04.033.

462 **Hèou M. B., Benjamin R., Jörg H., Kodjovi S. E., Abel A., Kpérkouma W. 2017.** Bayesian trend analysis
463   in annual rainfall total, duration and maximum in the Kara River basin (West Africa). Journal of
464   Hydrology: Regional Studies 13, 255–273. DOI 10.1016/j.ejrh.2017.08.009.

465 **Holben, B.N., 1986.** Characteristics of maximum-value composite images from temporal AVHRR data.
466   Int. J. Remote Sens. 7: 1417–1434. DOI 10.1080/01431168608948945.

467 **Hu, C.J., Fu, B.J., Liu, G.H., Jin, T.T., Guo, L., 2010.** Vegetation patterns influence on soil microbial
468   biomass and functional diversity in a hilly area of the Loess Plateau, China. J. Soil Sediment. 10(6):
469   1082–1091. DOI 10.1007/s11368-010-0209-3.

470 **IPCC, 2014.** The Synthesis Report (SYR) of the IPCC Fifth. *Available at*
471   https://archive.ipcc.ch/report/ar5/syr/.

472 **Ji L, Gallo K, Eidenshink J C. 2008.** Agreement evaluation of AVHRR and MODIS 16-day composite
473   NDVI datasets [J]. International Journal of Remote Sensing, 29(16): 4839-4861

474 **John S., Thomas V.W., Christopher F., 2015.** Probabilistic programming in Python using PyMC3. Peer J,
475   DOI 10.7717/peerj-cs.55.

476 **Jonsson, P. and Eklundh, L., 2002.** Seasonality extraction by function fitting to time-series of satellite
477   sensor data. IEEE T. Geo. sci. Remote. 40(8):1824-1832. DOI: 10.1109/TGRS.2002.802519.

478 **Kelly, M., Tuxen, K.A., Stralberg, D., 2011.** Mapping changes to vegetation pattern in a restoring
479   wetland: finding pattern metrics that are consistent across spatial scale and time. Ecol. Indic. 11(2):
480   263–273. DOI 10.1016/j.ecolind.2010.05.003.

481 **Kong, D.D., Zhang, Q., Huang, W.L, Gu, X.H., 2017.** Vegetation phenology change in Tibetan Plateau
482   from 1982 to 2013 and its related meteorological factors. Acta Geogr. Sin. 72(1): 39-52.

483 **Li G.Y., Jiang, C., Cheng, T., Bai J., 2019.** Grazing alters the phenology of alpine steppe by changing the
484   surface physical environment on the northeast Qinghai-Tibet Plateau, China. Journal of
485   Environmental Management, 248,109257. DOI 10.1016/j.jenvman.2019.07028.

486 **Li, H., Renssen, M., Roche, M., 2019.** Global vegetation distribution driving factors in two dynamic
487   global vegetation models of contrasting complexities. Global and Planetary Change, 180,51-56. DOI
488   10.1016/j.gloplacha.2019.05.009.

489 **Li, L.H., Zhang, Y.L., Wu, J.S., Li, S.C., Zhang, B.H., Zu, J.X., Zhang, H.M., Ding, M.J., Paudel, B., 2019.**
490   Increasing sensitivity of alpine grasslands to climate variability along an elevational gradient on the
491   Qinghai-Tibet Plateau. Science of the total environment, 678, 21-29. DOI
492   10.1016/j.scitotenv.2019.04.399.

493 **Li, Y.F., Li, Z.W., Wang, Z.Y., Wang, W.L., Ji, Y.H., Tian, S.M., 2017.** Impacts of artificially planted
494   vegetation on the ecological restoration of movable sand dunes in the Mugetan Desert, northeastern
495   Qinghai-Tibet Plateau. Int. J. Sediment Res. 32(2):277-287. DOI 10.1016/j.ijsrc.2017.02.003.

496 **Li, Z.W., Wang, Z.Y., Brierley, G., Nicoll, T. Pan, B.Z., Li, Y.F, 2015.** Shrinkage of the Ruoergai
497   Swamp and changes to landscape connectivity, Qinghai-Tibet Plateau. Catena, 126, 155–
498   163. DOI 10.1016/j.catena.2014.10.035.

499 **Liu, D., Cao, C.X., Olena Dubovyk, T, R., C, W., Z, Q.F., Zhao, Y.J., Gunter Menz, 2017.** Using fuzzy
500   analytic hierarchy process for spatio-temporal analysis of eco-environmental vulnerability change
501   during 1990–2010 in Sanjiangyuan region, China. Ecol. Indic. 73: 612-625. DOI
502   10.1016/j.ecolind.2016.08.031.

503 **Liu, Z, J., Wu, C. Y., Liu, Y. S., Wang, X. Y., Fang, B., Yuan, W. P., Ge, Q. S., 2017.** Spring green-up date
504   derived from GIMMS3g and SPOT-VGT NDVI of winter wheat cropland in the North China Plain.
505   ISPRS J. Photogramm. 130: 81-91. DOI 10.1016/j.isprsjprs.2017.05.015.

506 **Madden, H. 1978.** Comments on the Savitzky – Golay convolution method for least-squares fit smoothing
507   and differentiation of digital data. Analytical Chemistry, 50(9): 1383 – 1386.

508 **NASA-NEX, 2019.** *Available at* https://nex.nasa.gov/nex/projects/1349/

509 **Peng, J., Liu, Z.H., Liu, Y.H., Wu, J.S., Han, Y.A., 2012.**Trend analysis of vegetation dynamics in Qinghai–
510   Tibet Plateau using Hurst Exponent. Ecol. Indic. 14(1): 28-39. DOI 10.1016/j.ecolind.2011.08.011.

511 **Peter P., Bradley R., Dennis P. Watson, P. H., Marion S. 2018.** Greened Fentanyl related overdose in
512 Indianapolis: Estimating trends using multilevel Bayesian models. Addictive Behaviors 86, 4-10. DOI
513 10.1016/j.addbeh.2018.03.010.

514 **Piao, S., Fang, J., 2003.** Seasonal changes in vegetation activity in response to climate changes in China
515 between 1982 and 1999. Acta Geogr. Sin. 58(1), 119–125.

516 **Piao, S.L., Cui, M.D., Chen, A.P., Wang, X.H., 2011.** Altitude and temperature dependence of change in
517 the spring vegetation green- up date from 1982 to 2006 in the Qinghai-Xizang Plateau. Agr. Forest
518 Meteorol. 151(12): 1599-1608. DOI 10.1016/j.agrformet.2011.06.016.

519 **PROBA-V Products User Manual-Version: 3.01, 2018.**

520 **Rong, X.D., Bo, T., Kun, T., Yang, Y., 2010.** Landscape patterns and their changes in Sichuan
521 Ruoergai Wetland National Nature Reserve. Acta Ecological Sinica, 30, 27–32. DOI
522 10.1016/j.chnaes.2009.12.005

523 **Savitzky, A., & Golay, M. J. E. 1964.** Smoothing and differentiation of data by simplified least squares
524 procedures. Analytical Chemistry, 36: 1627 – 1639.

525 **Shen, G., Yang, X.C., Jin, Y.X., Xu, B., Zhou, Q.B., 2019.** Remote sensing and evaluation of the
526 wetland ecological degradation process of the Zoige Plateau Wetland in China. DOI
527 10.1016/j.ecolind.2019.04.063.

528 **Shen, M., Piao, S., Dorji T., 2016.** Plant phenological responses to climate change on the Tibetan Plateau:
529 Research status and challenges. Natl. Sci. Rev. 2(4): 454-467. DOI 10.1093/nsr/nwv058.

530 **Shen, M., Sun, Z., Wang, S., 2013.** No evidence of continuously advanced green-up dates in the Tibetan
531 Plateau over the last decade. P. Natl. Acad. Sci. USA. 110(26): E2329. DOI 10.1073/pnas.1304625110.

532 **Shen, M.G., Zhang, G.X., Cong, N., Wang, S.P., 2014.** Increasing altitudinal gradient of spring vegetation
533 phenology during the last decade on the Qinghai–Tibetan Plateau. Agr. Forest Meteorol. 189-190: 71-
534 80. DOI 10.1016/j.agrformet.2014.01.003.

535 **Steinier, J., Termonia, Y., & Deltour, J. 1972.** Comments on smoothing and differentiation of data by
536 simplified least squares procedure. Analytical Chemistry, 44(11): 1906 – 1909.

537 **Tang, Z.G., Ma, J.H., Peng, H.H., Wang, S.H., Wei, J.F., 2018.** Spatiotemporal changes of vegetation and
538 their responses to temperature and precipitation in upper Shiyang river basin. Adv. Space Res.
539 60(15): 969-979. DOI 10.1016/j.asr.2017.05.033.

540 **Torrence C, Compo G P., 1998.** A practical guide to wavelet analysis. B. Am. Meteorol. Soc. 79(1), 61-68

541 **Tucker, C.J., 1979.** Red and photographic infrared linear combinations for monitoring vegetation. Remote
542 Sens. Environ. 8(2): 127–150. DOI 10.1016/0034-4257(79)90013-0.

543 **Vegetation Index and Phenology Lab., The University of Arizona (VIP Lab.), 2011**. Available at
544 https://vip.arizona.edu.

545 **VITO, 2018. SPOT vegetation FAQ (frequently asked questions).** *Available at* VITO, 2018. SPOT
546 vegetation FAQ (frequently asked questions)

547 **Wang, X., Yao, Y.F., Alexandra H. Wortley., 2018.**Vegetation responses to the warming at the Younger
548 Dryas-Holocene transition in the Hengduan Mountains, southwestern China. Quaternary Sci. Rev.
549 192: 236-248. DOI 10.1016/j.quascirev.2018.06.007.

550   **Wu, C.Y., Peng, D.L, Kamel Soudani, Lukas Siebicke, 2017.** Land surface phenology derived from
551   normalized difference vegetation index (NDVI) at global FLUXNET sites. Agr. Forest Meteorol. 233:
552   171-182. DOI 10.1016/j.agrformet.2016.11.193.

553   **Yang, Y., Piao, S., 2006.** Variations in grassland vegetation cover in relation to climatic factors on the
554   Tibetan Plateau. J. Plant Ecol-China. 30(1), 1–8 .

555   **Yavuz Selim Guclu, 2018.** Multiple sen-innovative trend analyses and partial Mann-Kendall test. Journal
556   of Hydrology,566, 685-704. DOI 10.1016/j.jhydrol.2018.09.034.

557   **Yu, H., Luedeling, E. and Xu, J., 2010.** Winter and spring warming result in delayed spring phenology on
558   the Tibet plateau. P. Natl. Acad. Sci. USA. 107(51): 22151-22156. DOI 10.1073/pnas.1012490107.

559   **Zhang, G., Zhang, Y., Dong, J., 2013.** Green-up dates in the Tibetan Plateau have continuously advanced
560   from 1982 to 2011. P. Natl. Acad. Sci. USA. 110(11): 4309-4314. DOI 10.1073/pnas.1210423110.

561   **Zhao, K.G., Michael A. Wulder, Hu T, Ryan B., Wu, Q.S., Qin, H.M., Li, Y., Elizabeth T, Bani M,**
562   **Zhang, X.S., Molly B., 2019.** Detecting change-point, trend, and seasonality in satellite time series
563   data to track abrupt changes and nonlinear dynamics: A Bayesian ensemble algorithm. Remote
564   sensing of Environment, 232,111181 DOI 10.1016/j.rse.2019.04.034.

565   **Zheng, Y.T., Han, J.C., Huang, Y.F., Steven R. Fassnacht, Xie, S., Enze Lv, Chen, M., 2017.** Vegetation
566   response to climate conditions based on NDVI simulations using stepwise cluster analysis for the
567   Three-River Headwaters region of China. Ecol. Indic. 92: 18-29. DOI 0.1016/j.ecolind.2017.06.040.

Figure 1

Geographical location (A), land use and land cover (B, GLC2015), and the digital elevation model (C, STRM-30m) of the study area.

A) Geographical location. (B) Land use and land cover (GLC 2015). (C) Digital elevation model (STRM 30m)
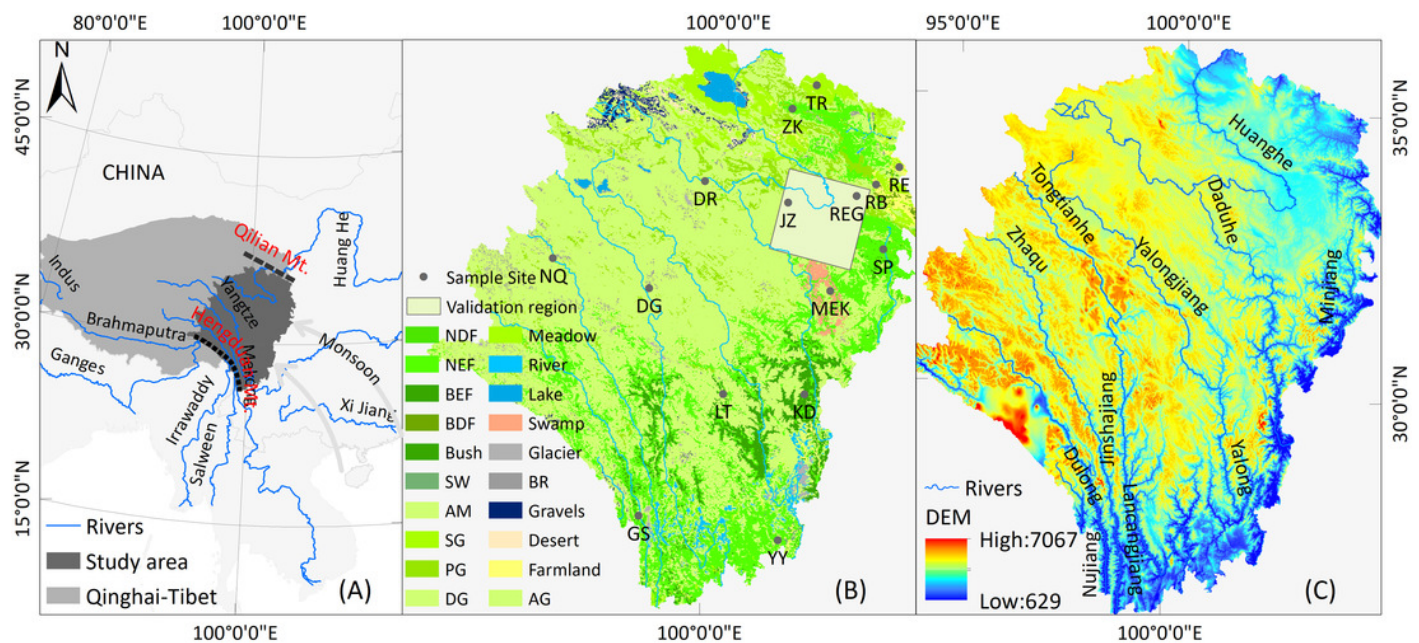
Figure 2

Vegetation cover types of sample site in study area.

(A) NQ, (B) DG, (C) REG, (D) TR, (E) GS, (F) YY, (G) LT, and (H) SP.

Note: The photographer is Haijun Wang.
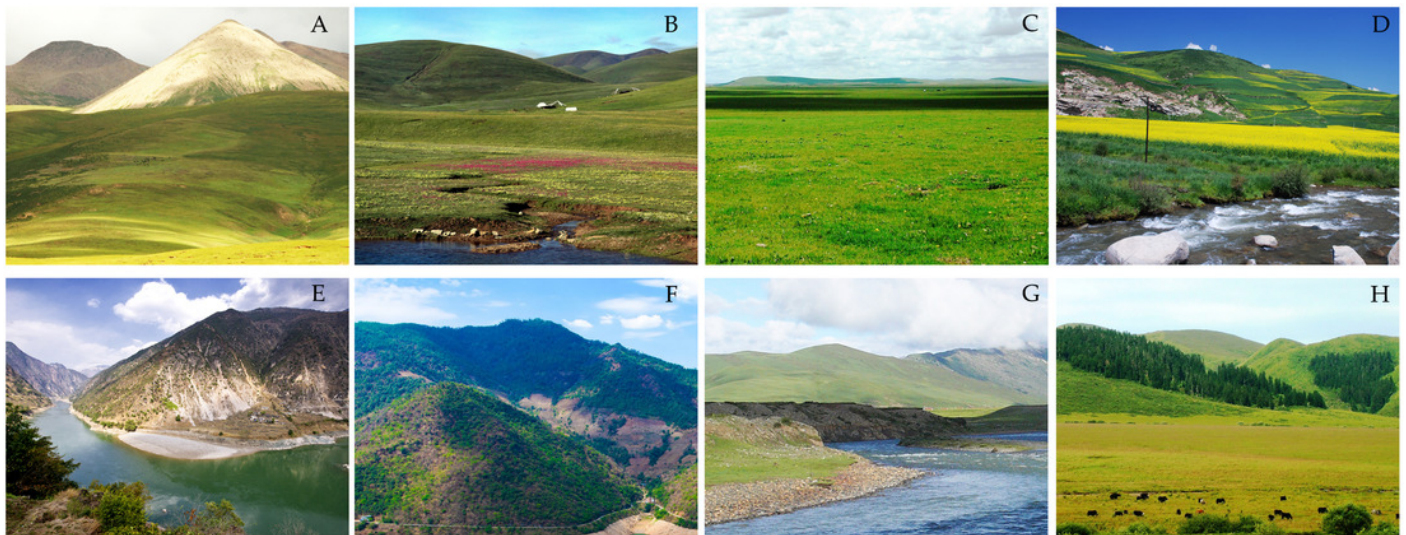
Figure 3

Schematic diagram of sample statistics.
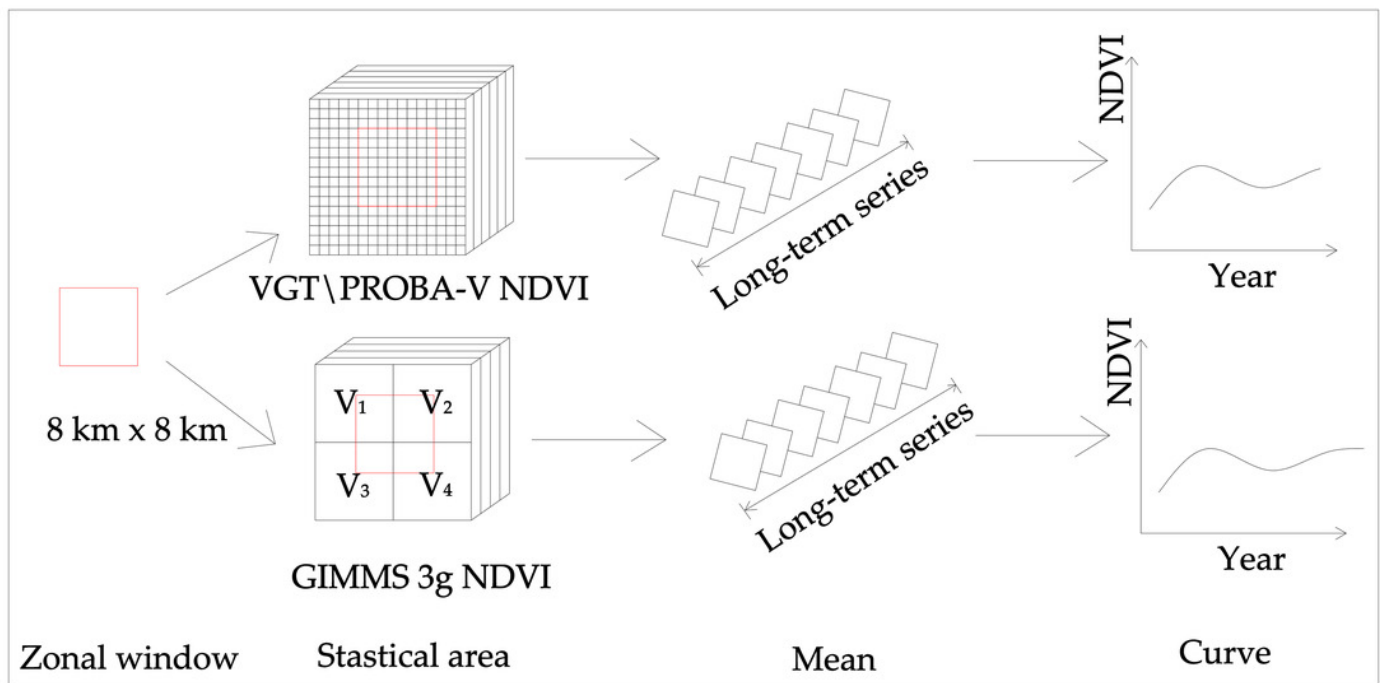
Figure 4

The trend and the confidence level of NDVI change based on the Bayesian method. Note: Beta (β) represents the continuous probability of trend change.
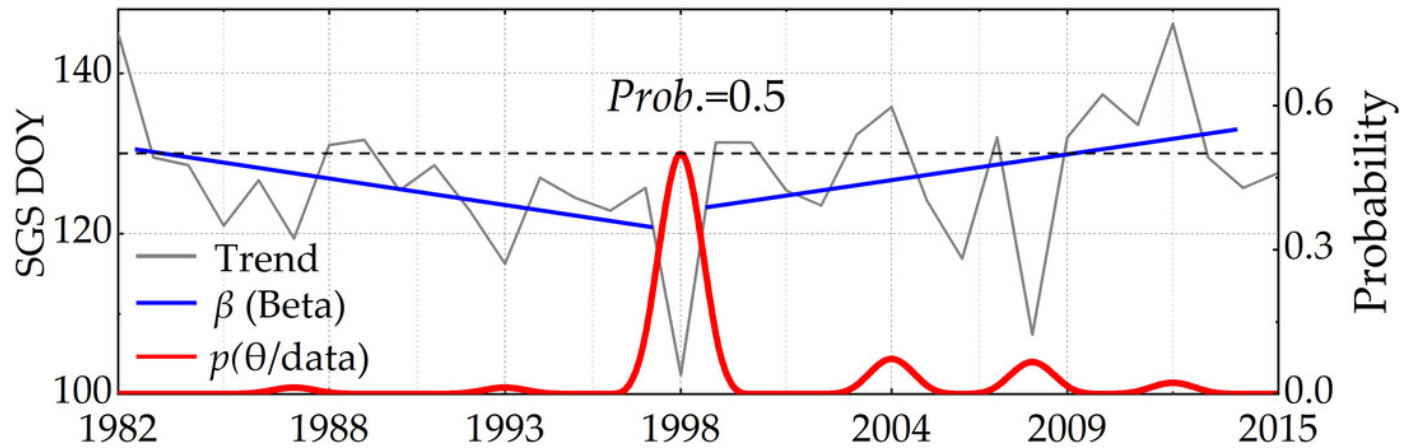
Figure 5

Flowchart of methodology used in this study.
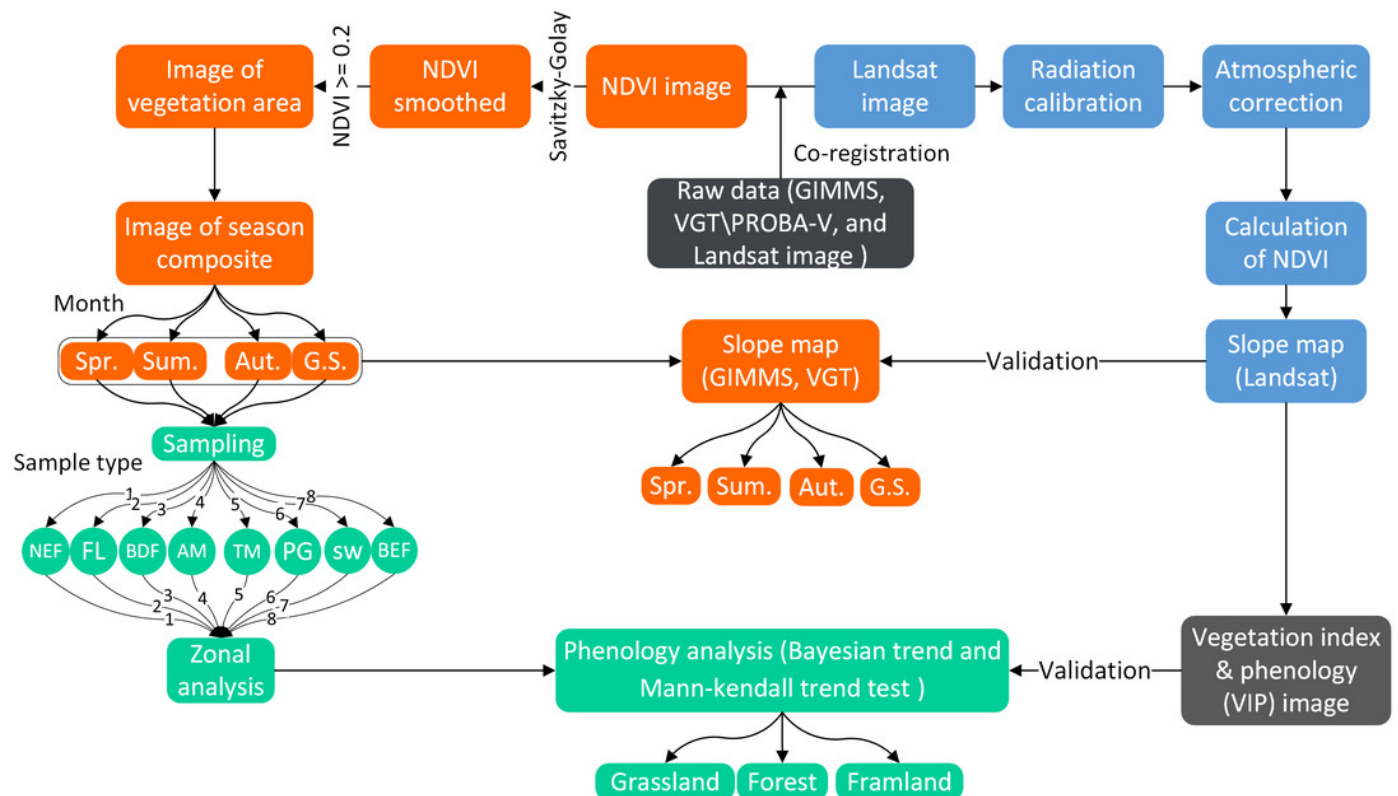
Figure 6

Trend and test of SGS and EGS from 1999 to 2018. The gray background area is the standard deviation (SD).

(A) Farmland. (B) Forest. (C) Grassland. (D) Farmland. (E) Forest. (F) Grassland. (G) Farmland. (H) Forest. (I) Grassland. (J) Farmland. (K) Forest. (L) Grassland.
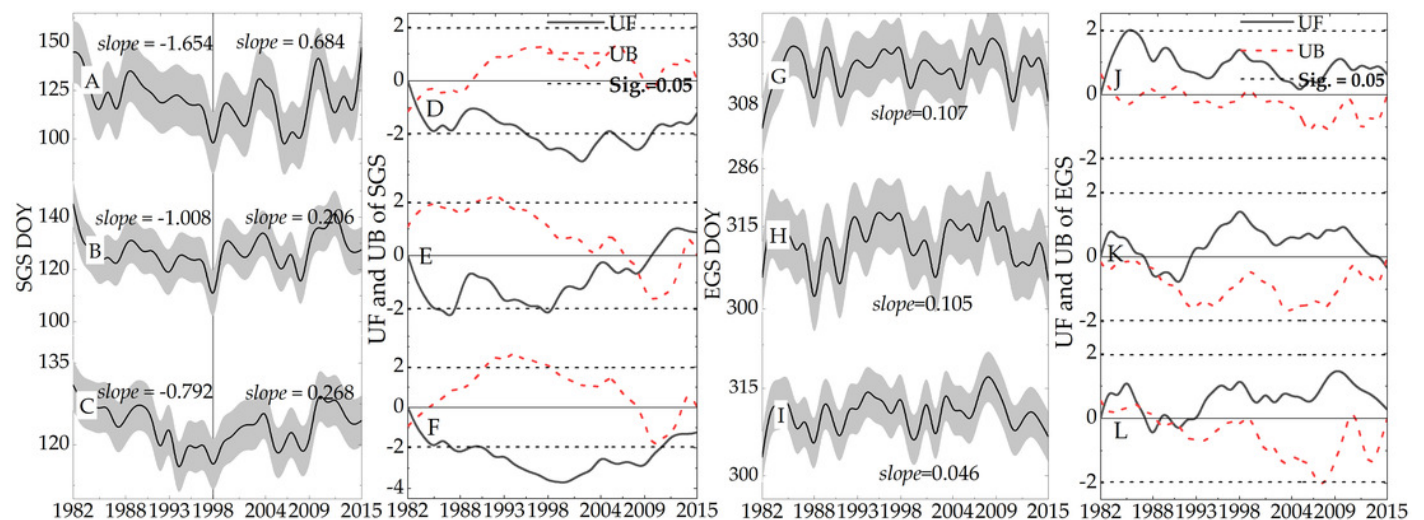
Figure 7

Spatial distribution of the vegetation dynamics from 1982 to 2015.

(A) Spring. (B) Summer. (C) Autumn. (D) Growing season.
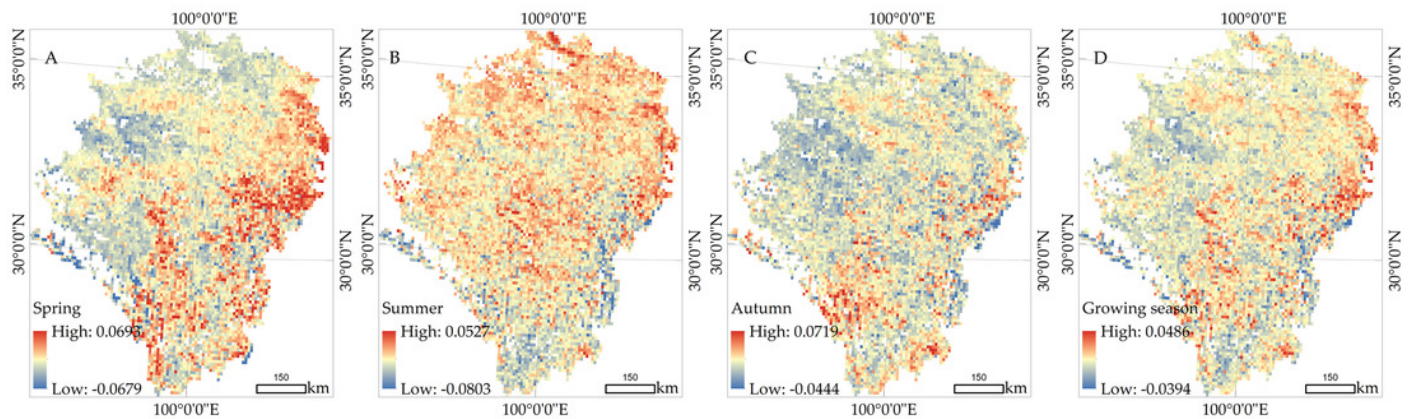
Figure 8

Spatial distribution of the vegetation dynamics from 1999 to 2015.

(A) Spring. (B) Summer. (C) Autumn. (D) Growing season. (E) Spring. (F) Summer. (G) Autumn. (H) Growing season.
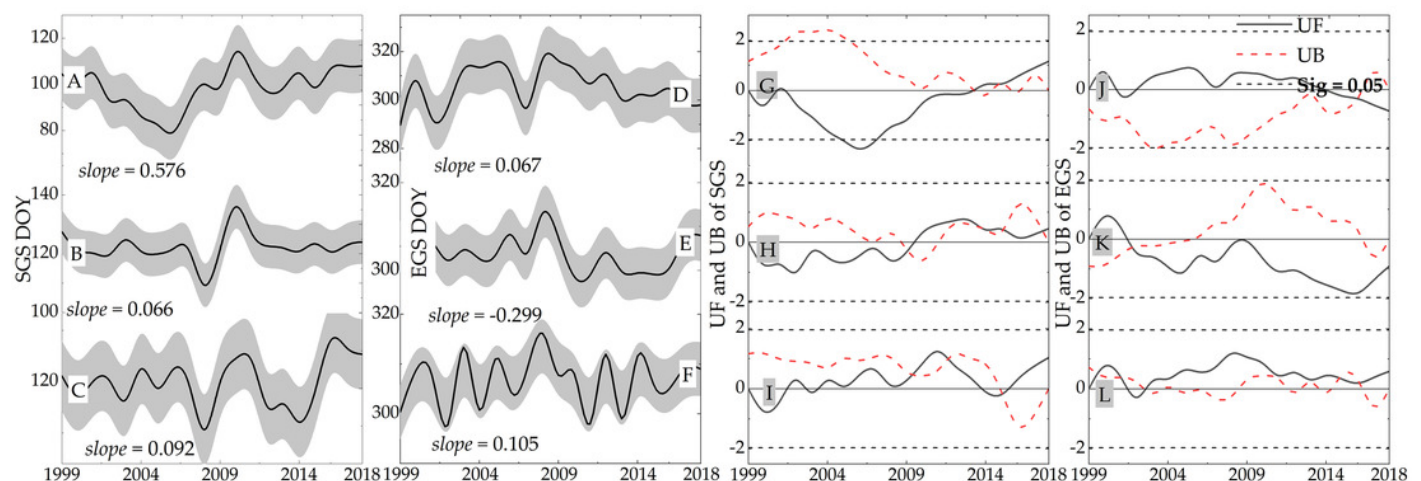
Figure 9

Spatial distribution of the vegetation dynamics in different seasons from 1999 to 2018.

(A) Spring. (B) Summer. (C) Autumn. (D) Growing season.
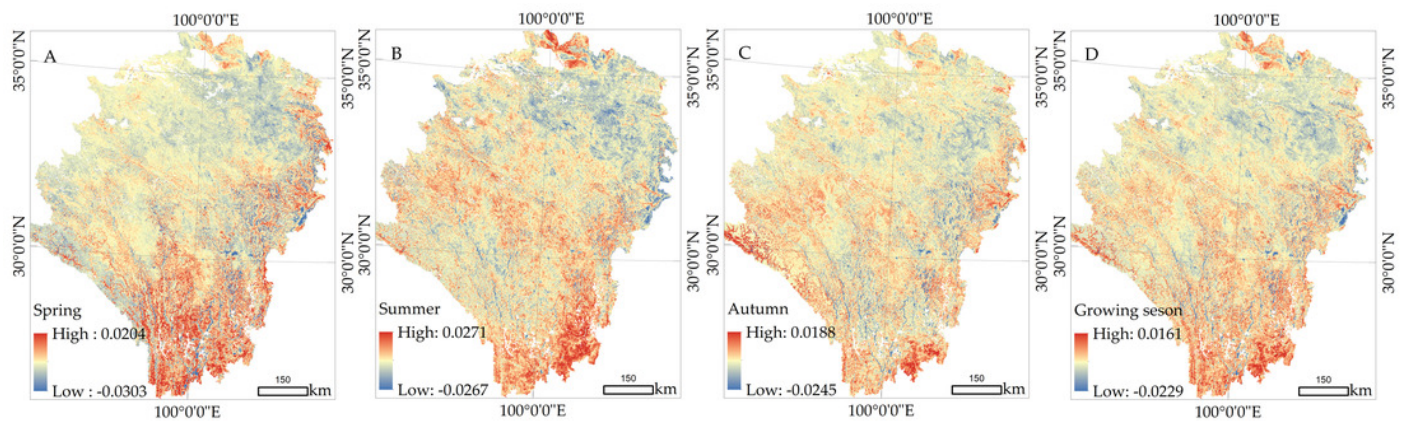
Figure 10

Spatial distribution of the vegetation dynamics from 1999 to 2015.

(A) Spring. (B) Summer. (C) Autumn. (D) Growing season. (E) Spring. (F) Summer. (G) Autumn. (H) Growing season.
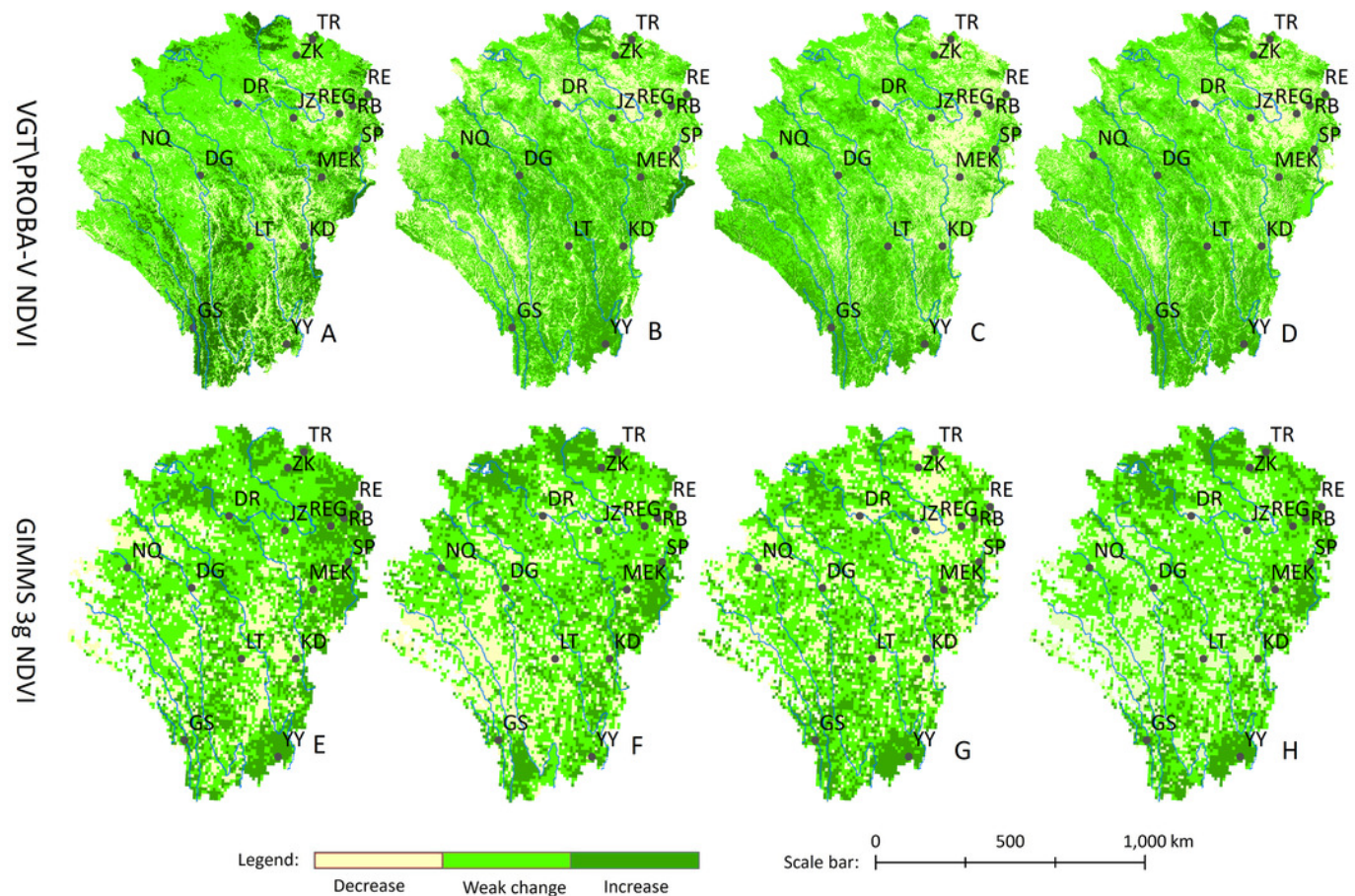
Figure 11

Trend of different vegetation at a site scale from 1999 to 2015.

(A) Spring. (B) Summer. (C) Autumn. (D) Growing season. (E) Spring. (F) Summer. (G) Autumn. (H) Growing season.
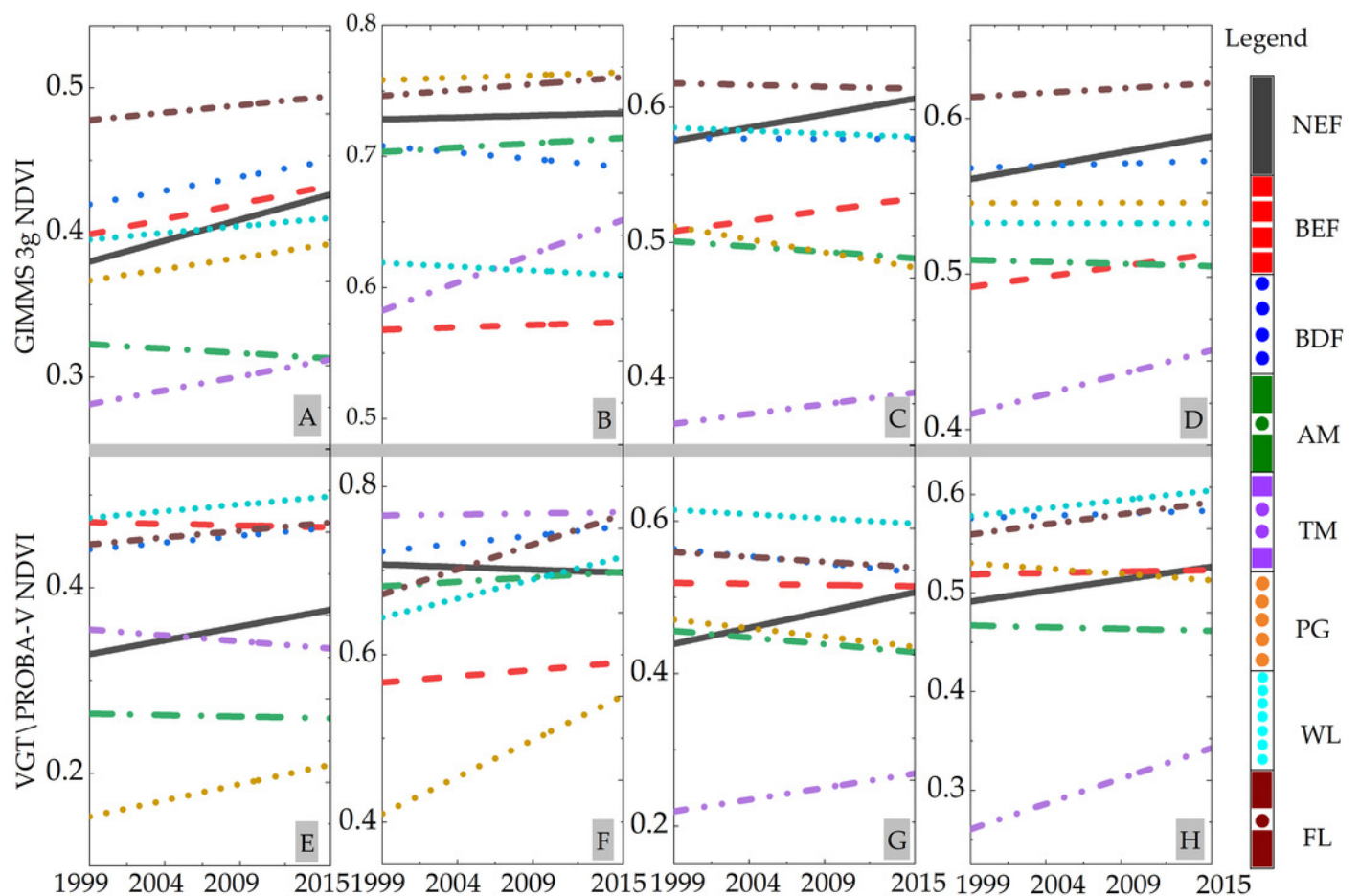
Figure 12

The trend and the confidence level of phenologicalchanges based on the Bayesian method.

Note: Blue solid line represents the continuous probability of trend change. Red solid line indicates the moment and probability of turning point occurring. Grey solid line denotes the change trend of raw data.

(A) Farmland. (B) Forest. (C) Grassland. (D) Farmland. (E) Forest. (F) Grassland.
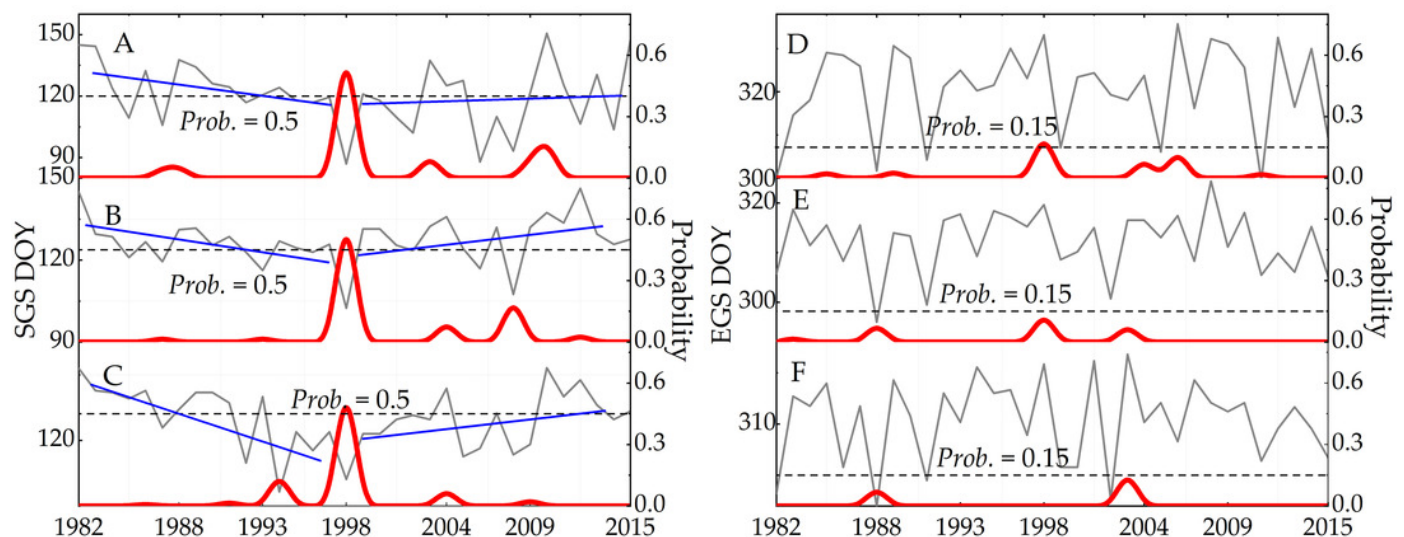
Figure 13

Using the data engine of VIP Lab to generate the global three-dimensional phenological grid (yearly product), including the start of growing season (SGS) and end of growing season (EGS).

Note: The data is a grid of spherical surface, and we only showed the section of the study area and surrounding areas.

(A), (B), (C) Spatial distribution of SGS. (D), (E), (F) Spatial distribution of EGS.
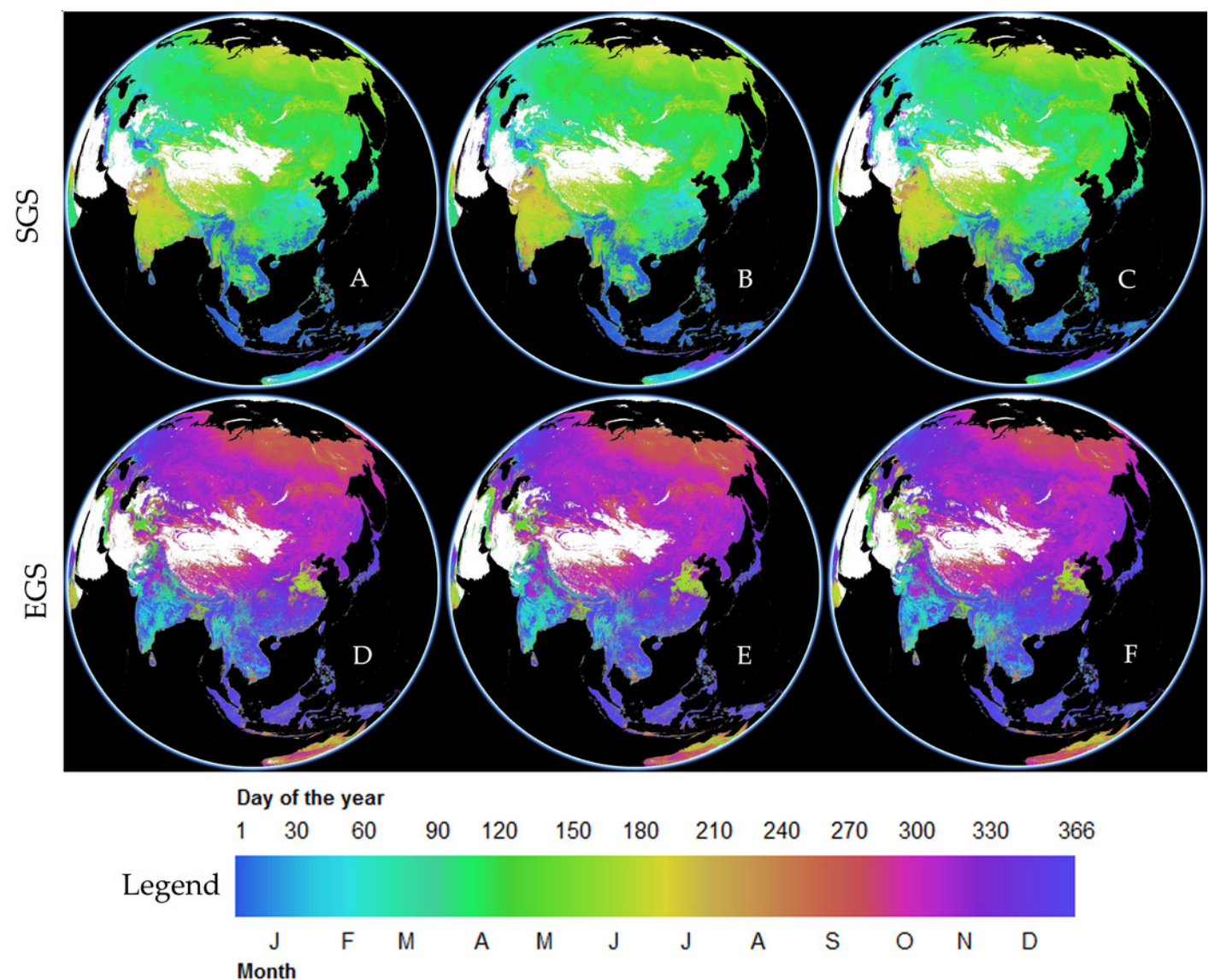
Figure 14

SGS and EGS of various vegetations were extracted from the VIP phenological grid, and the value extracted was used to validate the GIMMS 3g NDVI-based phenological changes in specific year.

(A) 1982. (B) 1998. (C) 2015.
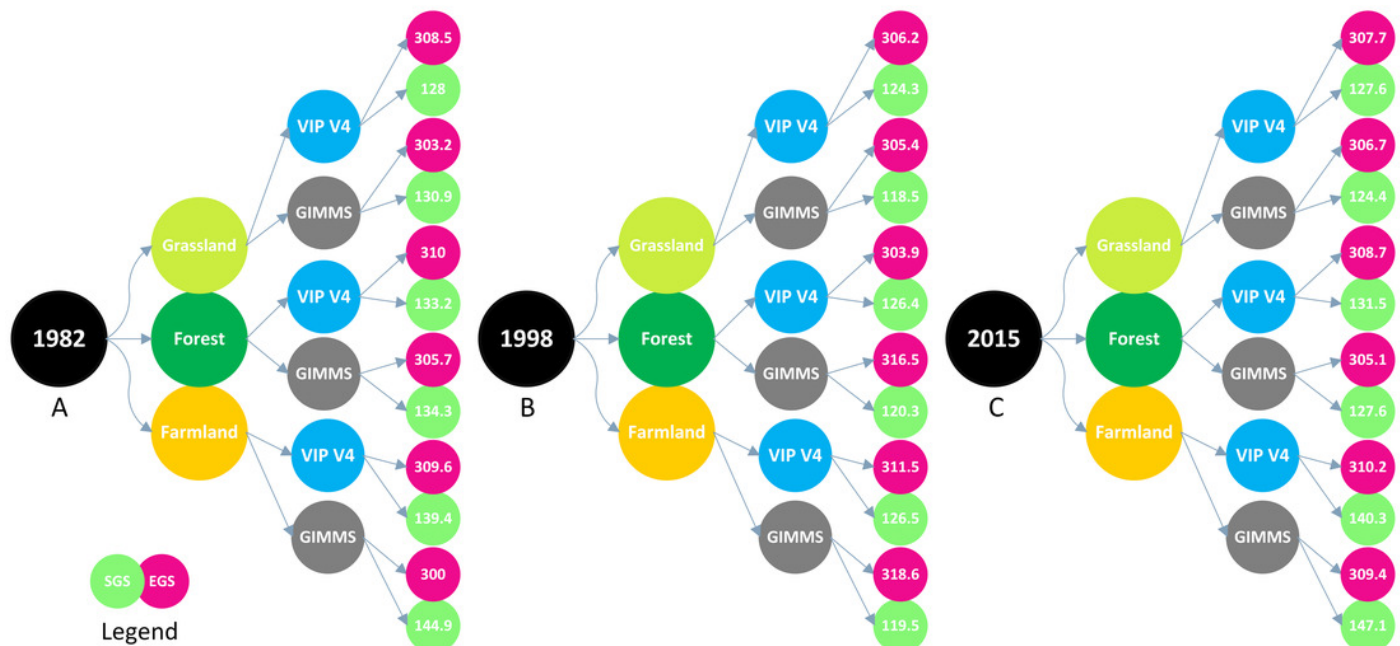
Figure 15

Validation of the vegetation dynamics from 1999 to 2015. A, B, and C is the slope of VGT\PROBA-V NDVI, the slope of Landsat NDVI, and true color image of Landsat OLI (2015/10/01), respectively.

(A) Slope of VGT NDVI. (B) Slope of Landsat NDVI. (C) Landsat 8 OLI image. (D) Site 1. (E) Site 2. (F) Site 3. (G) Site 4. (H) Site 5. (I) Site 1. (J) Site 2. (K) Site 3. (L) Site 4. (M) Site 5.
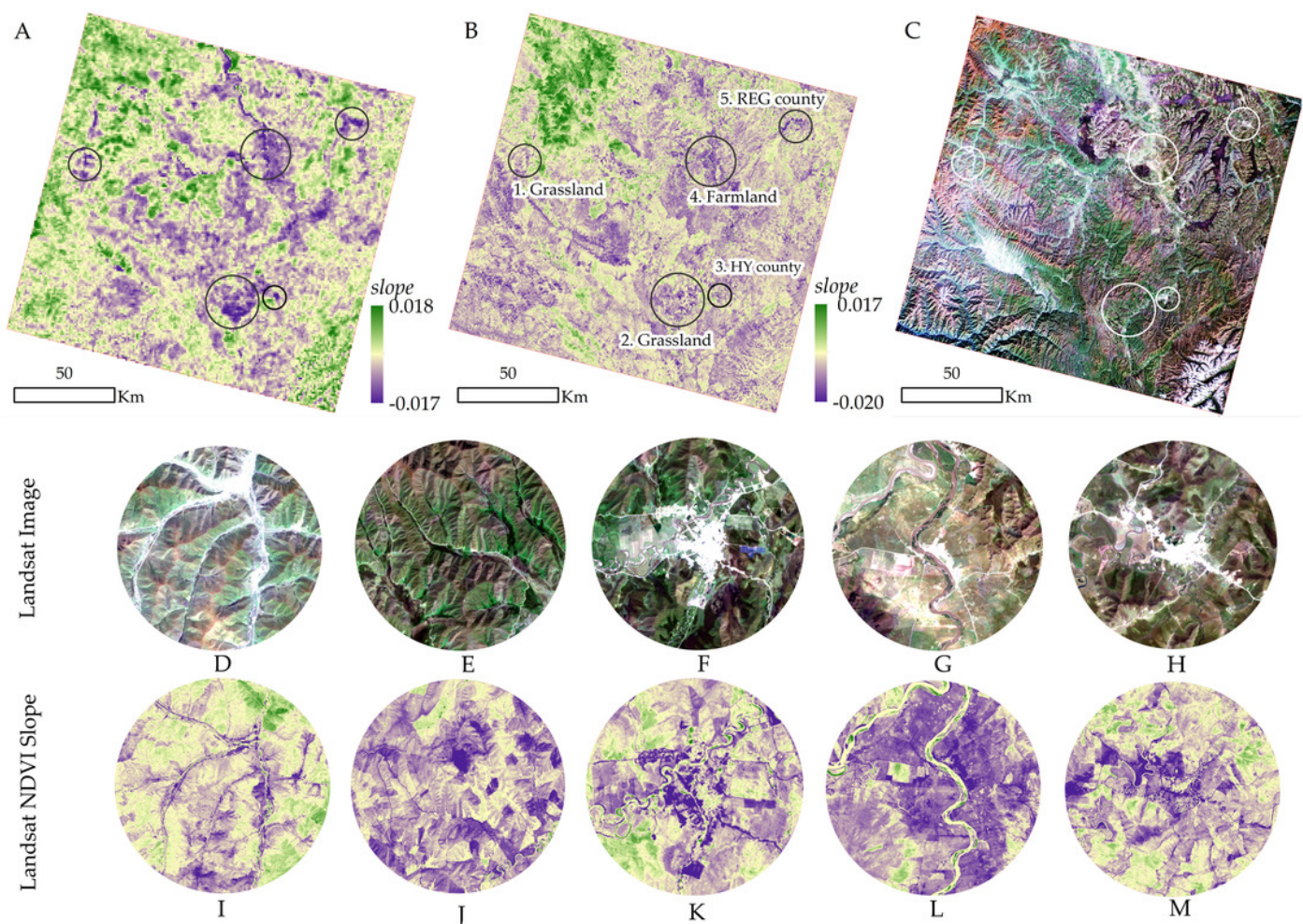
Acquisition date and sensor of Landsat orthophotoused in this study

Tab. 1 Acquisition date and sensor of Landsat orthophoto used in this study

Path/Row	131/37									
Sensor	Landsat 5 TM								Landsat 8 OLI	
Date (y/m/d)	1999/09/29	2000/10/04	2001/10/10	2003/09/28	2005/10/03	2007/09/27	2008/10/03	2011/10/06	2013/10/06	2015/10/01
Resolution	30 m									

Vegetation types and their use of the sample site.

Tab. 2. Vegetation types and their use of the sample site

Site	Longitude (°E)	Latitude (°N)	Altitude (m)	Vegetation type	Data use
Songpan (SP)	103.567	32.650	3732	Needle-leave deciduous forest (NEF)	Phenology analysis and vegetation dynamic
Ruobei (RB)	103.894	34.105	3155	Broadleaved deciduous forest (BDF)	Vegetation dynamic
Zeku (ZK)	101.504	35.094	3889		
Gongshan (GS)	98.667	27.750	2297		
Yanyuan (YY)	101.517	27.433	2571		
Kangding (KD)	101.967	30.050	4038	Broadleaved evergreen forest (BEF)	Vegetation dynamic
Litang (LT)	100.267	30.000	4581		
Jiuzhi (JZ)	101.483	33.433	3985	Alpine meadow (AM)	Phenology analysis and vegetation dynamic
Drerong (DR)	99.650	33.750	4396		
Nangqian (NQ)	96.483	32.20	3661		
Tongren (TR)	103.389	33.796	3164	Typical meadow (TM)	Vegetation dynamic
Dege (DG)	98.583	31.800	3918		
Ruoergai (REG)	102.967	33.583	3444	Plain grassland (PG)	Vegetation dynamic
Maerkang (MEK)	102.451	31.896	4708	Swamp (SW)	Vegetation dynamic
Ruoe (RE)	102.017	35.517	3229	Farm land (FL)	Phenology analysis and vegetation dynamic